Deep Learning-Based Detection of Epileptiform Discharges for Self-Limited Epilepsy With Centrotemporal Spikes

Yonghoon Jeon, Yoon Gi Chung, Taehyun Joo, Hunmin Kim, Hee Hwang, and Ki Joong Kim

***Abstract*— Centrotemporal spike-waves (CTSWs) are typical interictal epileptiform discharges (IEDs) observed in centrotemporal regions in self-limited epilepsy with centrotemporal spikes (SLECTS). This study aims to develop a deep learning-based approach for automated detection of CTSWs in scalp electroencephalography (EEG) recordings of patients with SLECTS. To lower the substantial burden of IED annotation on clinicians, we simplified it by limiting IEDs to CTSWs because electroencephalographic patterns of CTSWs are known to be highly consistent. Two neurologists annotated 1672 CTSWs of 20 patients with SLECTS. Thereafter, we performed a two-level CTSW detection procedure: epoch-level and EEG-level. In the epoch-level detection, we constructed convolutional neural network-based classification models for CTSW and non-CTSW binary classification using the recordings of 20 patients and 20 controls. We then set the thresholds of the classification models for 100% specificity. In the EEG-level detection, we applied the threshold-adjusted classification models to the recordings of 50 patients and 50 controls that were not used in the epoch-level detection to distinguish between CTSW-positive (with one or more CTSWs) and CTSW-negative (with no CTSW) recordings based on the detection of CTSW presence. We obtained an average sensitivity, specificity, and accuracy of 99.8%, 98.4%, and 99.1%, respectively, with an average false detection rate of 0.19/hr for the controls. Our approach showed high detectability for CTSWs despite the simplified annotation process. We expect that the proposed CTSW detectors have potential clinical usefulness for efficiently reading EEGs and diagnosing SLECTS, and can significantly reduce the burden of IED annotation on clinicians.**

***Index Terms*— Deep learning, electroencephalography (EEG), interictal epileptiform discharge (IED), self-limited epilepsy with centrotemporal spikes (SLECTS), spike detection.**

I. Introduction

EPILEPSY is a disorder characterized by recurrent unprovoked seizures resulting from abnormal brain activity such as neuronal hyperexcitability and hypersynchrony [1], [2], [3]. It has a worldwide prevalence of 0.64% [4], ranking third among neurological disorders in the global burden of disease study 2015 [5]. Various neuroimaging techniques, such as magnetic resonance imaging (MRI) and computed tomography, are utilized to examine epileptogenic lesions [6], [7]. However, electroencephalography (EEG) is required as an initial key step in the diagnosis of epilepsy to find evidences of cerebral abnormalities by monitoring electrophysiological brain activity [8], [9].

Interictal epileptiform discharges (IEDs) are transient neurophysiological activities with distinct morphological patterns on EEG recordings [10]. IEDs have been established as one of the diagnostic biomarkers for various epilepsy syndromes owing to their strong association with neurological pathologies and unique, syndrome-specific appearance on EEG recordings [1], [11]. However, considerable time and several tedious tasks are required to manually detect IEDs. Additionally, manual IED detection is highly dependent on clinicians' experience. Therefore, various conventional machine learning methods based on feature extraction via EEG signals processing in time and frequency domains have been proposed to automatically detect IEDs [12], [13], [14]. Recently, deep learning techniques with no handcrafted features have been suggested for automated end-to-end IED detection.

Most deep learning-based approaches use convolutional neural networks (CNNs) [15], [16], [17], [18], [19], [20],

Manuscript received 17 March 2022; revised 17 August 2022 and 13 October 2022; accepted 15 October 2022. Date of publication 19 October 2022; date of current version 27 October 2022. This work was supported by the Seoul National University Bundang Hospital Research Fund under Grant 14-2021-0046. *(Yonghoon Jeon and Yoon Gi Chung contributed equally to this work.) (Corresponding author: Hunmin Kim.)*

This work involved human subjects or animals in its research. Approval of all ethical and experimental procedures and protocols was granted by the Institutional Review Board (IRB) of the Seoul National University Bundang Hospital under IRB No. B-2106-688-105, and performed in line with the Declaration of Helsinki Principles.

Yonghoon Jeon is with the Department of Pediatrics, Seoul National University College of Medicine, Seoul National University Bundang Hospital, Seongnam, Gyeonggi-do 13620, South Korea, and also with the Graduate School of Data Science, Seoul National University, Seoul 08826, South Korea (e-mail: yonghoon.jhun@gmail.com).

Yoon Gi Chung and Hunmin Kim are with the Department of Pediatrics, Seoul National University College of Medicine, Seoul National University Bundang Hospital, Seongnam, Gyeonggi-do 13620, South Korea (e-mail: uskeywest@naver.com; hunminkim@snubh.org).

Taehyun Joo is with the Seoul National University College of Medicine, Seoul 08826, South Korea (e-mail: veritaspie@gmail.com).

Hee Hwang is with the Department of Pediatrics, Seoul National University College of Medicine, Seoul National University Bundang Hospital, Seongnam, Gyeonggi-do 13620, South Korea, and also with the Kakao Healthcare, Pangyo, Gyeonggi-do 13620, South Korea (e-mail: epilepsyguy@gmail.com).

Ki Joong Kim is with the Department of Pediatrics, Seoul National University College of Medicine, Seoul National University Children's Hospital, Seoul 08826, South Korea (e-mail: pednr@plaza.snu.ac.kr).

This article has supplementary downloadable material available at https://doi.org/10.1109/TNSRE.2022.3215526, provided by the authors.

Digital Object Identifier 10.1109/TNSRE.2022.3215526

[21], [22], [23], [24], recurrent neural networks (RNNs) [21], [25], [26], and hybrid methods [16], [21], [27] to identify IEDs on the scalp [15], [16], [17], [18], [19], [20], [21], [25], [27] and intracranial [22], [23], [24], [26] EEG recordings. To enhance IED detection ability, some studies further considered modification of conventional CNN architectures to extract spatial EEG features effectively from multiple scalp regions [7], [9]; multi-level morphological features and multi-channel co-occurrences of IEDs in deep neural networks [10]; augmentation of synthetic IEDs using a generative adversarial network [19]; a combination of template-matching and CNN approaches [18]; and visualization techniques to examine important areas of input data in time [13] and time-frequency [18] domains. RNNs can be adopted to capture temporal properties in long time series data [8], [10], [11]. Still, CNNs are widely used for the automated IED detection due to their convenience to handle high dimensional data such as multi-channel EEG recordings [12]. CNNs are also used to detect IEDs from simultaneous EEG and functional MRI recordings. However, the approach using EEG-functional MRI recordings is less effective than that using EEG owing to signal deterioration within MRI scanners [28].

Previous studies on deep learning-based automated IED detection used IEDs with various electroencephalographic patterns such as spikes, polyspike-waves, spike-waves, and sharp-waves to train classification models [15], [16], [22], [23], [26], [27]. Annotation of such IEDs can be extremely time-consuming, labor-intensive, and clinician-dependent because clinicians must carefully examine the various patterns in EEG recordings. This substantial burden on clinicians for IED annotation can be a potential obstacle for developing practical automated IED detectors owing to various reasons, such as an insufficient number of annotated IEDs and high inter-rater variability.

Self-limited epilepsy with centrotemporal spikes (SLECTS) — formerly known as benign epilepsy with centrotemporal spikes or benign rolandic epilepsy — is one of the most common childhood epilepsy syndromes [29], [30]. IEDs in interictal EEG recordings of patients with SLECTS are distinctly visible in centrotemporal regions [29], [31]. Therefore, they are called centrotemporal spike-waves (CTSWs). Clinical confirmation of CTSW presence in EEG recordings is crucial for diagnosing SLECTS [31]. The electroencephalographic patterns of CTSWs include a sharp transient peak followed by a trough and a slow wave with a horizontal dipole [32]. The CTSW patterns have morphological signatures; therefore, they can appear highly consistent with each other in EEG recordings. Considering these characteristics of CTSWs, clinicians should probably examine the consistent patterns during IED annotation, instead of the diverse patterns as suggested in previous studies, to develop IED detectors that exclusively examine CTSWs in EEG recordings of patients with SLECTS. Thus, we can simplify IED annotation if we focus on detecting specific IEDs.

In this study, we aimed to develop an automated IED detection approach specifically for detecting CTSWs in scalp EEG recordings of patients with SLECTS. We (1) adopted a deep learning technique to achieve high detectability without handcrafted feature extraction; (2) limited IEDs to CTSWs to lower the burden on clinicians for IED annotation; and (3) evaluated the clinical usefulness of the proposed CTSW detectors based on the discrimination of EEG recordings with at least one or more CTSWs and those with no CTSW.

II. Methods

A. Patients and Study Design

This retrospective study was approved by the Institutional Review Board (IRB) of the Seoul National University Bundang Hospital (IRB No. B-2106-688-105) and was conducted in accordance with the Declaration of Helsinki Principles. The IRB waived the requirement of informed consent owing to the retrospective nature of the study. The scalp EEG recordings of 70 patients with SLECTS (28 females and 42 males with mean age $\pm$ standard deviation of 8.7$\pm$1.3 and 8.6$\pm$1.3 years, respectively) and 70 controls (43 females and 27 males with mean age $\pm$ standard deviation of 10.4$\pm$2.6 and 11.5$\pm$3.0 years, respectively) were analyzed in this study. The diagnosis of SLECTS was based on the International League Against Epilepsy criteria [33]. The controls were neurologically intact and confirmed to have not experienced an epileptic seizure. Patients whose EEG data showed a typical and benign course of SLECTS were included, whereas those that showed atypical progression [34], and had insufficient EEG data and short follow-up periods were excluded. CTSWs in patients' EEG data were identified at the time of the initial diagnosis of SLECTS. All EEG recordings were obtained using a 32-channel digital EEG system (Grass Telefactor Inc., West Warwick, Rhode Island, United States) for at least 30 min with a sampling frequency of 200 Hz, notch filter of 60 Hz, and 19 electrodes, in accordance with the international 10–20 system. If required, chloral hydrate (50 mg/kg, maximum 1000 mg) was used as a sedative. All signals were re-referenced to an average reference, and band-pass filtered between 1 and 70 Hz.

We performed a two-stage CTSW detection procedure comprising epoch- and EEG-level detections. The epoch-level detection was used to construct CNN-based classification models for CTSW and non-CTSW binary classification using the EEG recordings of 20 patients with SLECTS and 20 controls. Two pediatric neurologists (H. H. and H. K.) annotated CTSWs of the 20 patients. During CTSW annotation, each CTSW was defined from the beginning of its spike to the end of its wave component. Low-to-medium voltage spike-waves, spikes with no wave components, and spike-wave complexes overlapping or coinciding with artifacts were excluded. The EEG-level detection was performed to distinguish between EEG recordings with at least one or more CTSWs (hereinafter termed *CTSW-positive recordings*) and those with no CTSWs (hereinafter termed *CTSW-negative recordings*). The EEG-level discrimination was based on the detection of CTSW presence in the entire EEG recordings of 50 patients with SLECTS and 50 controls that were not used in epoch-level detection. Same neurologists confirmed the presence and absence of CTSWs in the recordings of patients and controls, respectively. Fig. 1 shows the overall process

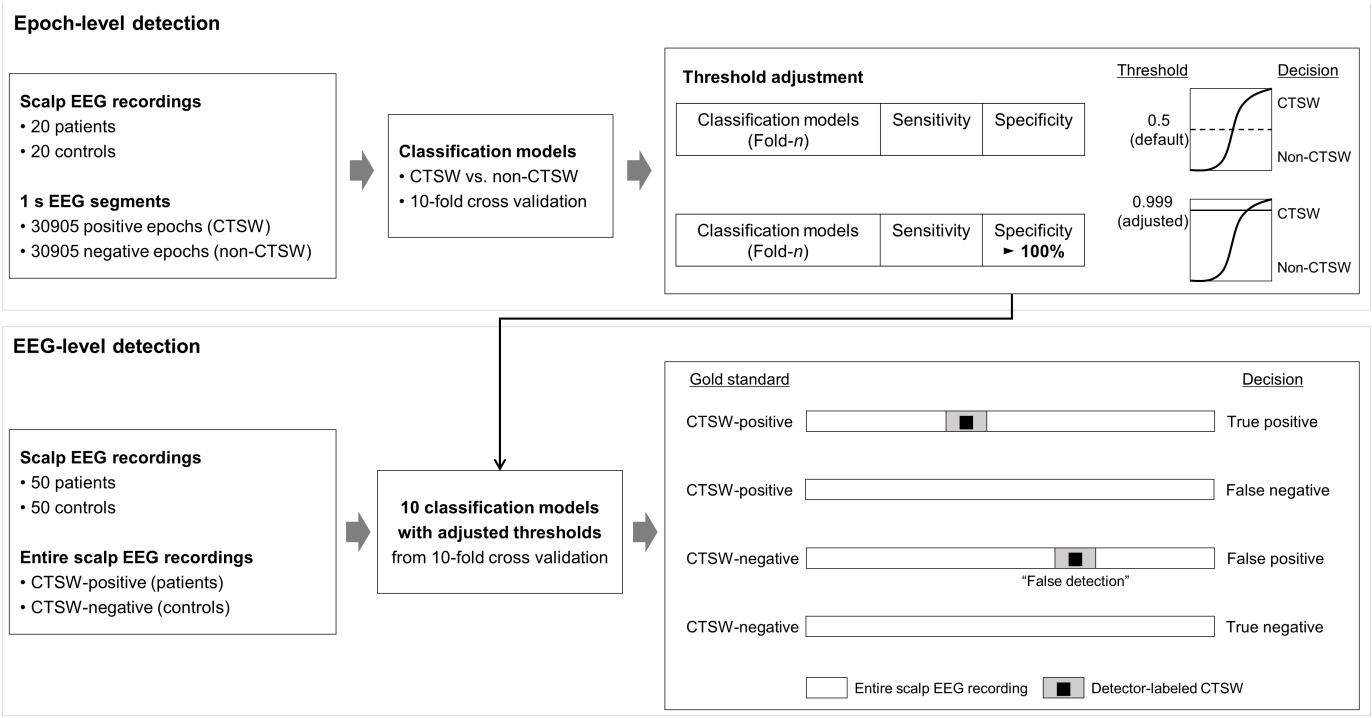

Fig. 1. Overall process from epoch-level to EEG-level detections. Epoch-level detection is to construct CNN-based classification models for CTSW and non-CTSW binary classification using the EEG recordings of 20 patients with SLECTS and 20 controls. Thresholds of the classification models are adjusted to have 100% specificity. EEG-level detection was to discriminate CTSW-positive and CTSW-negative recordings based on the identification of the presence of CTSWs over the entire EEG recordings, using the EEG recordings of 50 patients with SLECTS and 50 controls which were not handled in the previous epoch-level detection.

from the epoch-level to EEG-level detections (please refer to Supplementary Fig. S1 for more details).

B. Epoch-Level Detection

To prepare a dataset for feeding into our CNN-based classification models, we segmented the EEG recordings of 20 patients and 20 controls into 1 s epochs. The epoch length was determined based on the longest duration among annotated CTSWs, allowing each epoch to sufficiently contain the entire shape of a CTSW. The segments from the recordings of patients contained CTSWs (hereinafter termed *positive epochs*), whereas those from the recordings of controls did not (hereinafter termed *negative epochs*). To generate the positive epochs, we segmented the recordings of patients at starting points of individual CTSWs. To generate negative epochs, we segmented the recordings of controls at random time points. Same neurologists confirmed that the negative epochs contained no suspicious abnormal components. To handle imbalanced data distributions, horizontal flipping and jittering (-100, -50, 50, and 100 ms based on the center of each epoch) were applied to the positive epochs for data augmentation, whereas random undersampling was applied to the negative epochs. A total of 61810 epochs were obtained with a 1:1 ratio of positive and negative epochs. All the epochs from the EEG recordings of 20 patients and 20 controls were split into 80% and 20% for training and testing, respectively. Therefore, 48694 epochs from recordings of 16 patients and 16 controls were used for training, and 13116 from those of 4 patients and 4 controls were used for testing (please refer to Supplementary Fig. S1 for more details).

True positives were positive epochs with CTSWs; false negatives were those with no CTSW; false positives were negative epochs with CTSWs; and true negatives were those with no CTSW. We measured the performance of the classification models based on sensitivity, specificity, and accuracy using 10-fold cross validation and acquired 10 classification models. The sensitivity, specificity, and accuracy were defined as the number of true positives divided by the number of positive epochs, number of true negatives divided by the number of negative epochs, and number of correctly classified epochs divided by the total number of epochs, respectively. To maximize the ability to distinguish negative epochs, we adjusted the default threshold of 0.5 for the classification models such that they had 100% specificity. Hence, we acquired 10 threshold-adjusted classification models (CTSW detectors) for subsequent EEG-level detection. We evaluated the performance of the threshold-adjusted classification models based on their sensitivities and accuracies.

C. EEG-Level Detection

To distinguish between CTSW-positive and CTSW-negative recordings, we applied the threshold-adjusted classification models to the EEG recordings of 50 patients and 50 controls that were not used in epoch-level detection. The threshold-adjusted classification models identified the presence of CTSWs across the entire EEG recording using a sliding window technique with a 1 s window and no overlap.

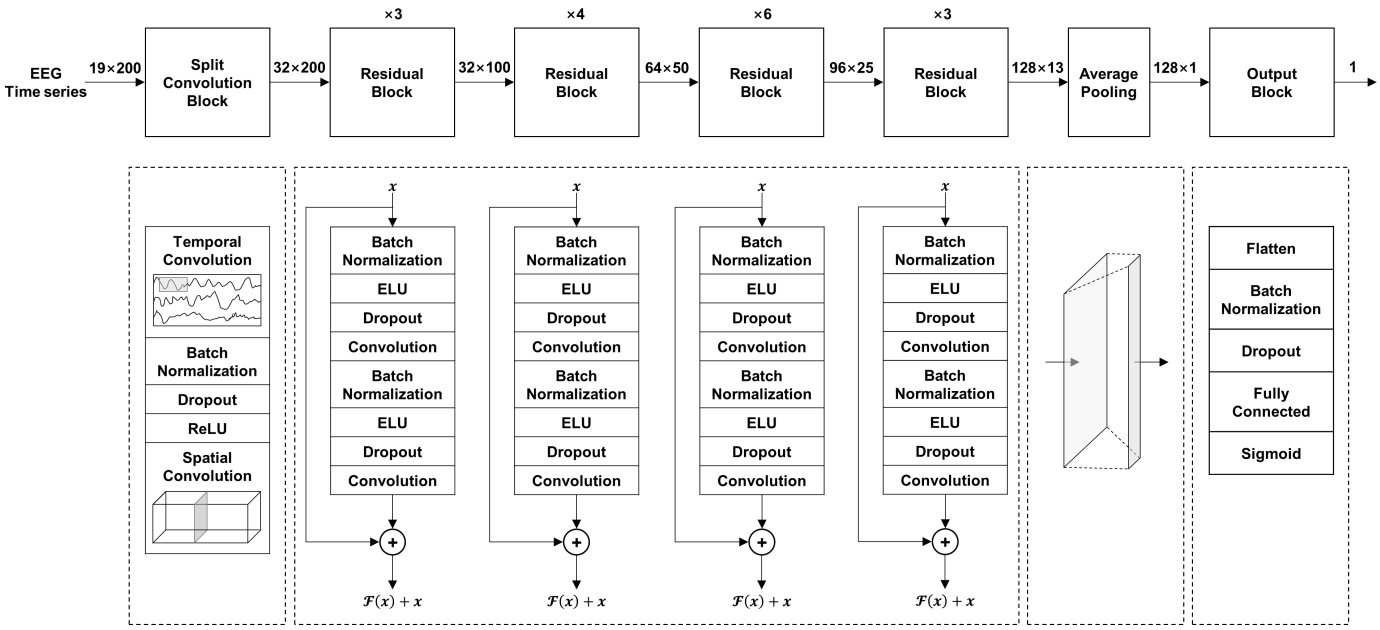

Fig. 2. Overall CNN architecture for CTSW detection. Multi-channel EEG time series with a size of 19 channels ×200 data points (1 s) are fed into the split convolution block consisting of temporal and spatial convolutions. After the split convolution block, 16 residual blocks are sequentially added with a total number of 32 convolution layers. Feature maps after the residual blocks and average pooling are fed into the output block for CTSW and non-CTSW binary classification using a sigmoid function. The total number of model parameters is 763105. (ReLU: rectified linear unit; ELU: exponential linear unit).

The CTSWs identified by the models were termed *detector-labeled CTSWs*.

True positives were CTSW-positive recordings with at least one or more detector-labeled CTSWs; false negatives were those with no detector-labeled CTSW; false positives were CTSW-negative recordings with at least one or more detector-labeled CTSWs; and true negatives were those with no detector-labeled CTSW. We termed all detector-labeled CTSWs in false positives as *false detections*. We measured the discrimination performance of the models based on their sensitivity, specificity, accuracy, and false detection rate (FDR). The sensitivity, specificity, and accuracy were defined as the number of true positives divided by the number of CTSW-positive recordings, number of true negatives divided by the number of CTSW-negative recordings, and number of correctly discriminated recordings divided by the total number of recordings, respectively. The FDR was defined as the number of false detections divided by the EEG recording time for each false positive. We measured the FDR only for the control recordings.

D. CNN Architecture

Our CNN architecture was adopted from previous studies [15], [35], [36]. It initialized from a split convolution block with a temporal convolution layer followed by a spatial convolution layer. The temporal convolution layer had a filter size of 1 × 5 and 32 linear units. The filter size of the spatial convolution layer was 19 × 32, where 19 and 32 were the numbers of channels and linear units in the previous temporal convolution layer, respectively. A rectified linear unit between the temporal and spatial convolution layers was used as the activation function.

After the split convolution block, we sequentially added 16 residual blocks with 32 convolution layers [36], [37]. Each residual block had two temporal convolution layers with a filter size of 1 × 3. We used two exponential linear units [38] as activation functions in each residual block. After the residual blocks, we added an output block with feature maps calculated through average pooling. The feature maps were flattened and fed into the fully connected layers. We used a sigmoid function for CTSW and non-CTSW binary classification.

We used batch normalization and dropout layers to prevent overfitting [39], [40], [41], He initializer to initialize weights for the convolution layers [42], early stopping to enhance training speed with a patience of 10, AMSGrad [43] and ReduceLROnPlateau [44] as optimization methods with an initial learning rate of 0.0003 and a patience of 5, and a binary cross-entropy loss function as the cost function. We set the number of training epochs to 50 with a batch size of 128.

We used PyTorch library 1.9.0 [44] with a NVIDIA 3080Ti (12GB) graphics processing unit and compute unified device architecture (CUDA) 11.4 programming interface. The entire CNN architecture is shown in Fig. 2.

III. Results

We obtained 1672 CTSWs from the scalp EEG recordings of 20 patients with SLECTS. On average, the number of CTSWs was 83.6±66.3 (mean ± standard deviation) for a 37.4±10.3 min recording time per patient (2.2±2.0 CTSWs/min). An epoch length of 1 s was determined based on the fact that the maximum durations of CTSWs ranged from 0.44–0.77 s. Detailed information on the patients and their CTSWs is presented in Table I. Fig. 3 shows representative positive and negative epochs.

TABLE I

PATIENT INFORMATION ON THE EPOCH-LEVEL DETECTION. A TOTAL NUMBER OF CTSWS OBTAINED FROM THE SCALP EEG RECORDINGS OF 20 PATIENTS WITH SLECTS IS 1672. ON AVERAGE, THE NUMBER OF CTSWS IS 83.6±66.3 (MEAN±SD, WHERE SD IS STANDARD DEVIATION) FOR 37.4±10.3 MIN RECORDING TIME PER PATIENT (2.2±2.0 CTSWS/MIN). THE MAXIMUM DURATIONS OF CTSWS RANGE FROM 0.44 TO 0.77 S

Subject No.	Age	Sex	Number of CTSW	Max. CTSW duration (s)	Min. CTSW duration (s)	EEG length (min)	CTSW/min
1	10.7	M	105	0.64	0.23	33.3	3.2
2	9.7	M	62	0.60	0.26	30.3	2.0
3	10.1	F	174	0.65	0.26	36.1	4.8
4	8.1	M	108	0.70	0.29	33.1	3.3
5	6.6	M	41	0.58	0.30	36.5	1.1
6	10.6	M	147	0.62	0.28	70.1	2.1
7	8.9	M	8	0.44	0.28	30.1	0.3
8	9.7	F	58	0.58	0.28	60.7	1.0
9	8.6	F	55	0.58	0.27	38.5	1.4
10	7.2	F	57	0.50	0.22	34.5	1.7
11	9.6	M	68	0.58	0.21	30.1	2.3
12	8.3	F	18	0.46	0.28	30.1	0.6
13	7.9	M	287	0.77	0.23	31.1	9.2
14	5.7	M	53	0.48	0.24	30.1	1.8
15	9.0	M	49	0.50	0.32	38.2	1.3
16	5.8	F	50	0.48	0.22	36.6	1.4
17	9.2	M	40	0.58	0.36	36.2	1.1
18	7.8	M	54	0.61	0.29	32.7	1.7
19	8.7	M	172	0.65	0.26	41.1	4.2
20	7.4	F	66	0.48	0.27	38.3	1.7
Total			1672			747.7	
Mean	8.5		83.6			37.4	2.2

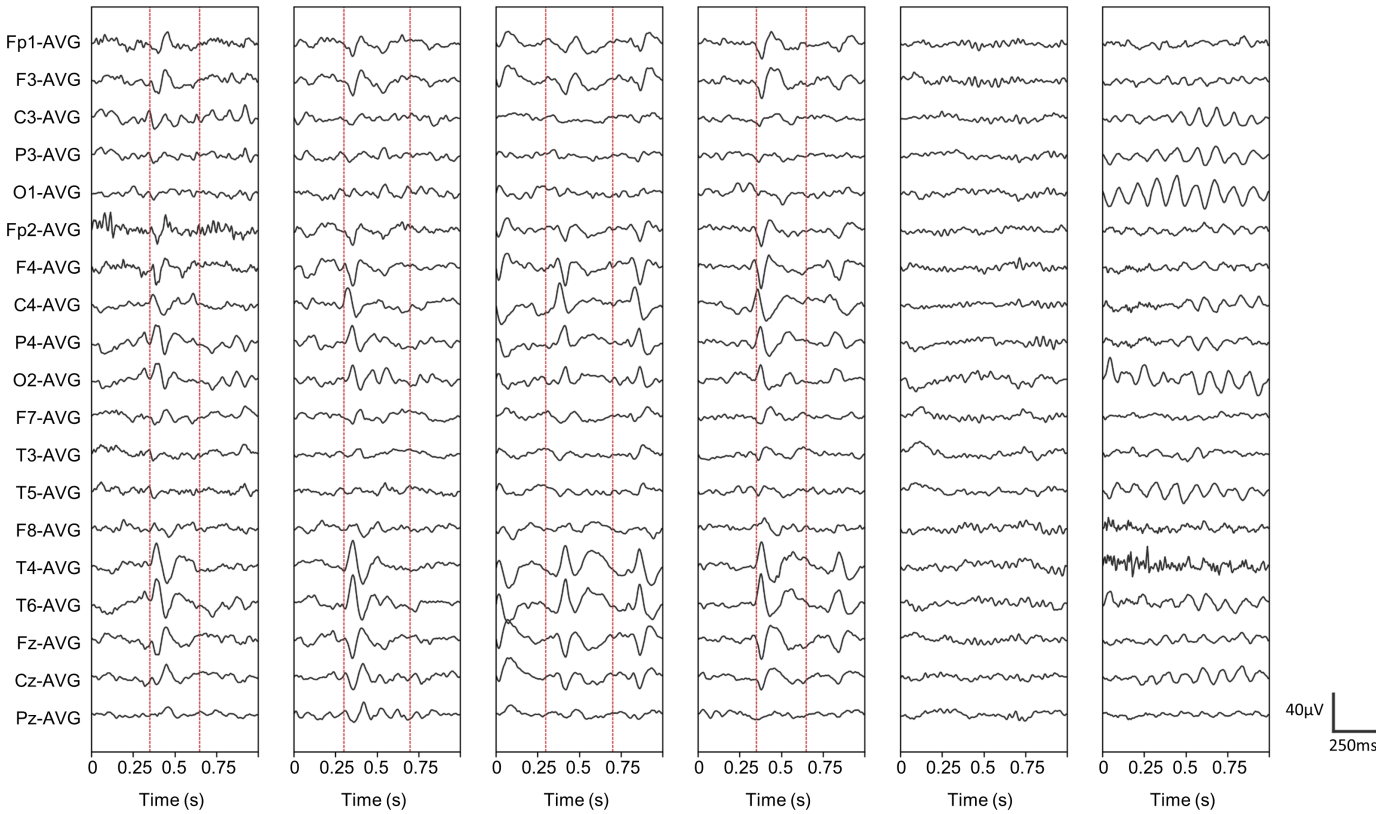

Fig. 3. Representative positive (CTSW) and negative (no CTSW) epochs in epoch-level detection. Subplots with two dotted lines show positive epochs. The first line indicates a starting point and the second line indicates an end point of each CTSW. Subplots with no line show negative epochs.

In the epoch-level detection, the proposed method obtained a sensitivity, specificity, and accuracy of 99.66±0.40%, 99.87±0.12%, and 99.83±0.15%, respectively, averaged over 10-fold cross validation runs for the classification of positive and negative epochs. We then adjusted the thresholds of the 10 classification models such that they had 100% specificity.

TABLE II

EPOCH-LEVEL DETECTION RESULTS ON THE EEG RECORDINGS OF 20 PATIENTS AND 20 CONTROLS. EPOCH-LEVEL DETECTION SHOWS A SENSITIVITY, SPECIFICITY, AND ACCURACY OF 99.66±0.40%, 99.87±0.12%, AND 99.83±0.15%, RESPECTIVELY, AVERAGED OVER THE 10-FOLD CROSS VALIDATION RUNS FOR THE CLASSIFICATION OF THE POSITIVE (CTSW) AND NEGATIVE (NON-CTSW) EPOCHS. A DEFAULT THRESHOLD OF 0.5 IS ADJUSTED FOR THE 10 CLASSIFICATION MODELS TO HAVE 100% SPECIFICITY. THE SENSITIVITY AND ACCURACY ARE CHANGED TO 85.82±5.65% AND 97.74±0.90%, RESPECTIVELY, WITH AN ADJUSTED THRESHOLD OF 0.9988±0.0008 AVERAGED OVER THE THRESHOLD-ADJUSTED CLASSIFICATION MODELS

Run (Model)	Sensitivity (%)	Specificity (%)	Accuracy (%)	Default threshold	Sensitivity (%)	Specificity (%)	Accuracy (%)	Adjusted threshold
1	99.81	99.89	99.88	0.5	85.58	100	97.70	0.9994
2	100	99.92	99.93	0.5	90.16	100	98.43	0.9989
3	99.67	99.96	99.92	0.5	87.11	100	97.94	0.9978
4	99.71	99.92	99.89	0.5	77.32	100	96.38	0.9997
5	99.90	99.80	99.82	0.5	95.75	100	99.32	0.9973
6	99.95	99.92	99.92	0.5	88.97	100	98.24	0.9994
7	99.00	99.91	99.76	0.5	82.86	100	97.26	0.9986
8	98.81	99.52	99.41	0.5	86.29	100	97.81	0.9982
9	99.76	99.92	99.89	0.5	75.74	100	96.13	0.9992
10	100	99.90	99.92	0.5	88.44	100	98.15	0.9992
Mean±SD	99.66±0.40	99.87±0.12	99.83±0.15	-	85.82±5.65	-	97.74±0.90	0.9988±0.0008

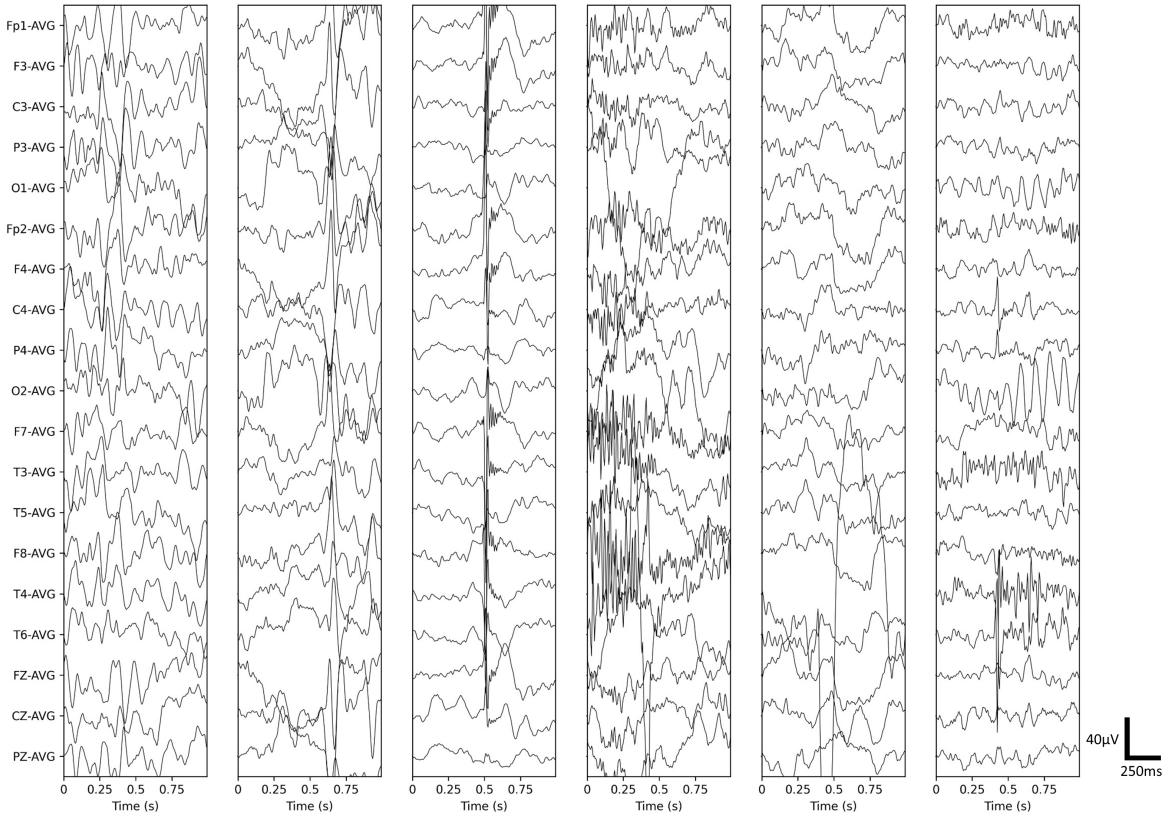

Fig. 4. Representative false detections by the fifth classification model in EEG-level detection. From left to right: vertex sharp transients, K-complexes, electrostatic artifacts, muscle artifacts, electrode pop artifacts, and a combination of electrostatic and muscle artifacts.

As a result, the proposed method obtained a sensitivity and accuracy of 85.82±5.65% and 97.74±0.90%, respectively, with an adjusted threshold of 0.9988±0.0008 averaged over the 10 threshold-adjusted classification models for subsequent EEG-level detection. Detailed results of the epoch-level detection are presented in Table II.

In the EEG-level detection, the proposed method obtained a sensitivity, specificity, and accuracy of 99.80±0.63%, 98.40±2.63%, and 99.10±1.29%, respectively, averaged over the 10 threshold-adjusted classification models for distinguishing between CTSW-positive and CTSW-negative recordings. On average, 49.9±0.3 (true positive) and 0.1±0.3 (false negative) recordings of 50 patients were classified as CTSW-positive and CTSW-negative, respectively, and 49.2±1.3 (true negative) and 0.8±1.3 (false positive) recordings of 50 controls were classified as CTSW-negative and CTSW-positive, respectively. Additionally, we observed an average FDR of 0.19±0.16/hr (6.5±5.5 false detections over

TABLE III

EEG-LEVEL DETECTION RESULTS ON THE EEG RECORDINGS OF 50 PATIENTS AND 50 CONTROLS. EEG-LEVEL DETECTION SHOWS A SENSITIVITY, SPECIFICITY, AND ACCURACY OF 99.80±0.63%, 98.40±2.63%, AND 99.10±1.29%, RESPECTIVELY, AVERAGED OVER THE THRESHOLD-ADJUSTED CLASSIFICATION MODELS FOR THE DISCRIMINATION OF CTSW-POSITIVE AND CTSW-NEGATIVE RECORDINGS. ON AVERAGE, 49.9±0.3 (TRUE POSITIVE) AND 0.1±0.3 (FALSE NEGATIVE) RECORDINGS OF 50 PATIENTS ARE CLASSIFIED AS CTSW-POSITIVE AND CTSW-NEGATIVE ONES, RESPECTIVELY. ON AVERAGE, 49.2±1.3 (TRUE NEGATIVE) AND 0.8±1.3 (FALSE POSITIVE) RECORDINGS OF 50 CONTROLS ARE CLASSIFIED AS CTSW-NEGATIVE AND CTSW-POSITIVE ONES, RESPECTIVELY

Model	EEG recordings of patients			EEG recordings of controls			Accuracy (%)
	True positive	False negative	Sensitivity (%)	False positive	True negative	Specificity (%)	
1	50	0	100	1	49	98	99
2	50	0	100	2	48	96	98
3	50	0	100	0	50	100	100
4	49	1	98	0	50	100	99
5	50	0	100	4	46	92	96
6	50	0	100	0	50	100	100
7	50	0	100	0	50	100	100
8	50	0	100	1	49	98	99
9	50	0	100	0	50	100	100
10	50	0	100	0	50	100	100
Mean±SD	49.9±0.3	0.1±0.3	99.80±0.63	0.8±1.3	49.2±1.3	98.40±2.63	99.10±1.29

34.1 hr recording time) for 50 controls. Each control showed an FDR from 0 to 2.56±1.66/hr (false detections from 0 to 1.6±2.0) averaged over the 10 threshold-adjusted classification models. Detailed results of the EEG-level and false detections are presented in Tables III and IV, respectively. Fig. 4 shows that the false detections by the fifth classification model included vertex sharp transients, K-complexes, and electrostatic, muscle, and electrode pop artifacts.

IV. DISCUSSION

In this study, we proposed and demonstrated a deep learning-based approach for automated detection of CTSWs from scalp EEG recordings of patients with SLECTS. To extract spatiotemporal features of CTSWs from EEG time series, we adopted a CNN architecture initialized with consecutive temporal and spatial convolutions. To lower the burden on clinicians during IED annotation, we limited IEDs to CTSWs because CTSWs have consistent electroencephalographic patterns. To evaluate the clinical usefulness of the proposed CTSW detectors, we performed EEG-level detection to distinguish between CTSW-positive and CTSW-negative recordings based on the detection of CTSW presence in the entire EEG recording. In the EEG-level detection, the proposed method obtained an average sensitivity, specificity, and accuracy of 99.80%, 98.40%, and 99.10%, respectively, with an average FDR of 0.19/hr for controls by using the threshold-adjusted classification models to reduce false detections.

Recent studies on deep learning-based automated IED detection have reported high IED and non-IED binary classification performance for scalp [15], [16], [17], [18], [19], [20], [21], [25], [27] and intracranial [22], [23], [24], [26] EEG recordings. Some studies further evaluated their approaches for distinguishing between EEG recordings with and without IEDs. They reported a sensitivity and specificity of 88.89% for 54 recordings with IEDs, and 69.57% for 46 recordings with no IED [17]; a specificity of 83.30% for 12 recordings with no IED [16]; and an area under the receiver operating characteristic curve (AUROC) of 0.847 (the number of EEG recordings was not provided) [15]. In this study, we termed this evaluation *EEG-level detection*. Some studies also examined the relationship between the sensitivity and false positive rates in IED and non-IED binary classification (epoch-level detection in this study). They reported a sensitivity of 97.0% for a false positive rate less than 6 per minute and 84.0% for less than 1 per minute [23], and a sensitivity of 96.7% for a false positive rate of 1.16 per minute and 85.0% for 0.14 per minute [18]. They implied that a sensitivity reduction could be required to reduce the number of false positives in IED and non-IED binary classification. Therefore, we adjusted the thresholds of our classification models such that they had 100% specificity to minimize the number of false positives in epoch-level detection. We expected our classification models to identify negative epochs more accurately with adjusted thresholds than with the default ones, thereby inducing low false detection rates in EEG-level detection. Our classification models had 100% specificity in the epoch-level detection. However, in the EEG-level detection, they made some false detections because the EEG recordings used were new data for them.

In the EEG-level detection, we distinguished between CTSW-positive and CTSW-negative recordings using the threshold-adjusted classification models to detect CTSW presence. This procedure is crucial for screening out the EEG recordings with no CTSW during the diagnosis of SLECTS. If the screening is successful, clinicians are required to only review the EEG recordings with CTSWs. Thus, we can expect an efficiency improvement for EEG readings in clinical environments. Because clinicians will review the EEG recordings with CTSWs regardless of the number of CTSWs, false detections in those recordings will have no effect on the EEG reading. However, because they can skip reading EEG recordings with no CTSW, no false detections in those recordings can reduce the number of recordings that must be reviewed [18].

In this study, we proposed a deep learning-based automated IED detection approach that can identify CTSWs in the scalp EEG recordings of patients with SLECTS. One of our

TABLE IV

THE OCCURRENCE OF FALSE DETECTIONS FOR 50 CONTROLS IN THE EEG-LEVEL DETECTION. 50 CONTROLS SHOW AN AVERAGE FDR OF 0.19±0.16/HR (6.5±5.5 FALSE DETECTIONS OVER 34.1 HR RECORDING TIME). EACH CONTROL SHOWS AN FDR FROM 0 TO 2.56±1.66/HR (FALSE DETECTIONS FROM 0 TO 1.6±2.0) AVERAGED OVER THE THRESHOLD-ADJUSTED CLASSIFICATION MODELS

Subject No.	EEG length (min)	EEG length (hr)	Number of false detections											FDR (/hr), Mean ± SD
			Threshold-adjusted classification model										Mean ± SD	
			1	2	3	4	5	6	7	8	9	10		
1	33.02	0.6	0	0	0	0	0	0	0	0	0	0	0.0±0.0	0.00±0.00
2	30.92	0.5	0	0	0	0	0	0	0	0	0	0	0.0±0.0	0.00±0.00
3	34.30	0.6	0	0	0	0	0	0	0	0	0	0	0.0±0.0	0.00±0.00
4	31.15	0.5	0	0	0	0	0	0	0	0	0	0	0.0±0.0	0.00±0.00
5	72.42	1.2	0	0	0	0	0	0	0	0	0	0	0.0±0.0	0.00±0.00
6	34.30	0.6	0	0	0	0	0	0	0	0	0	0	0.0±0.0	0.00±0.00
7	30.10	0.5	0	0	0	0	0	0	0	0	0	0	0.0±0.0	0.00±0.00
8	30.80	0.5	0	0	0	0	1	0	0	1	0	0	0.2±0.4	0.39±0.82
9	45.15	0.8	0	0	0	0	0	0	0	0	0	0	0.0±0.0	0.00±0.00
10	62.30	1.0	0	0	0	0	0	0	0	0	0	0	0.0±0.0	0.00±0.00
11	40.13	0.7	0	0	0	0	0	0	0	0	0	0	0.0±0.0	0.00±0.00
12	49.12	0.8	0	0	0	0	0	0	0	0	0	0	0.0±0.0	0.00±0.00
13	30.22	0.5	0	0	0	0	0	0	0	0	0	0	0.0±0.0	0.00±0.00
14	35.35	0.6	0	0	0	0	0	0	0	0	0	0	0.0±0.0	0.00±0.00
15	35.47	0.6	0	0	0	0	0	0	0	0	0	0	0.0±0.0	0.00±0.00
16	35.75	0.6	0	0	0	0	0	0	0	0	0	0	0.0±0.0	0.00±0.00
17	75.75	1.3	2	2	1	0	7	1	0	1	1	1	1.6±2.0	1.27±1.59
18	36.17	0.6	0	0	0	0	0	0	0	0	0	0	0.0±0.0	0.00±0.00
19	30.10	0.5	0	0	0	0	0	0	0	0	0	0	0.0±0.0	0.00±0.00
20	40.02	0.7	0	0	0	0	0	0	0	1	0	0	0.1±0.3	0.15±0.47
21	35.12	0.6	1	2	1	1	4	1	1	2	1	1	1.5±1.0	2.56±1.66
22	32.08	0.5	0	0	0	0	0	0	0	0	0	0	0.0±0.0	0.00±0.00
23	40.02	0.7	0	0	0	0	1	0	0	0	0	0	0.1±0.3	0.15±0.47
24	30.10	0.5	0	0	0	0	0	0	0	0	0	0	0.0±0.0	0.00±0.00
25	30.22	0.5	0	0	0	0	0	0	0	0	0	0	0.0±0.0	0.00±0.00
26	50.28	0.8	0	0	0	0	0	0	0	0	0	0	0.0±0.0	0.00±0.00
27	41.53	0.7	1	1	1	1	1	0	1	1	1	1	0.9±0.3	1.30±0.46
28	59.03	1.0	1	1	1	1	1	0	0	0	1	1	0.7±0.5	0.71±0.49
29	39.55	0.7	0	0	0	0	0	0	0	0	0	0	0.0±0.0	0.00±0.00
30	32.90	0.5	0	0	0	0	1	0	0	1	0	0	0.2±0.4	0.36±0.77
31	31.38	0.5	0	0	0	0	0	0	0	0	0	0	0.0±0.0	0.00±0.00
32	77.70	1.3	0	0	0	0	0	0	0	0	0	0	0.0±0.0	0.00±0.00
33	33.07	0.6	0	0	0	0	0	0	0	0	0	0	0.0±0.0	0.00±0.00
34	34.93	0.6	0	0	0	0	0	0	0	0	0	0	0.0±0.0	0.00±0.00
35	36.63	0.6	0	0	0	0	0	0	0	0	0	0	0.0±0.0	0.00±0.00
36	32.00	0.5	0	0	0	0	0	0	0	0	0	0	0.0±0.0	0.00±0.00
37	42.47	0.7	0	0	0	0	0	0	0	0	0	0	0.0±0.0	0.00±0.00
38	42.35	0.7	0	0	0	0	0	0	0	0	0	0	0.0±0.0	0.00±0.00
39	63.35	1.1	0	0	0	0	0	0	0	0	0	0	0.0±0.0	0.00±0.00
40	38.38	0.6	0	0	0	0	1	0	0	0	0	0	0.1±0.3	0.16±0.49
41	41.07	0.7	0	0	0	0	2	0	0	0	0	0	0.2±0.6	0.29±0.92
42	35.47	0.6	0	0	0	0	0	0	0	0	0	0	0.0±0.0	0.00±0.00
43	38.85	0.6	0	0	0	0	0	0	0	0	0	0	0.0±0.0	0.00±0.00
44	39.78	0.7	1	1	1	0	2	0	0	0	0	1	0.6±0.7	0.90±1.05
45	60.13	1.0	0	0	0	0	0	0	0	0	0	0	0.0±0.0	0.00±0.00
46	49.47	0.8	0	0	0	0	0	0	0	0	0	0	0.0±0.0	0.00±0.00
47	31.97	0.5	0	0	0	0	0	0	0	0	0	0	0.0±0.0	0.00±0.00
48	51.87	0.9	0	1	0	0	0	0	0	0	0	1	0.2±0.4	0.23±0.49
49	30.57	0.5	0	0	0	0	0	0	0	0	0	0	0.0±0.0	0.00±0.00
50	30.10	0.5	0	0	0	0	0	0	0	1	0	0	0.1±0.3	0.20±0.63
False detection			6	8	5	3	21	2	2	8	4	6	6.5±5.5	
FDR (/hr)			0.18	0.23	0.15	0.09	0.62	0.06	0.06	0.23	0.12	0.18	0.19±0.16	
Total length	2044.88	34.1												

aims was to alleviate the burden on clinicians during IED annotation, which can help avoid an obstacle for developing automated IED detectors. To solve this problem, we limited IEDs to CTSWs because they have consistent electroencephalographic patterns. Therefore, clinicians (two pediatric neurologists in this study) could focus on the consistent patterns in EEG recordings during IED annotation. Our approach has a limitation in that it can only be used for CTSW detection. However, it can simplify IED annotation and lower the workload of clinicians for CTSW detection. Previous IED detection

TABLE V
PERFORMANCE OF DEEP LEARNING-BASED AUTOMATED IED DETECTION IN PREVIOUS STUDIES AND CTSW DETECTION IN THIS STUDY

Reference	EEG type	Model	Performance		
			Epoch-level	Epoch-level (adjusted)	EEG-level
This study	scalp	Split CNN (Temporal + Spatial convolutions)	99.83% accuracy 99.66% sensitivity 99.87% specificity	97.74% accuracy 85.82% sensitivity (with 100% specificity)	99.80% sensitivity (50 recordings with CTSWs) 98.40% specificity (50 recordings without CTSWs) 0.19/hr FDR
S. Clarke et al (2021) [18]	scalp	CNN	96.7% sensitivity	85% sensitivity (with 0.14/min FDR)	
C. Lourenco et al (2019) [19]	scalp	CNN	93-99% sensitivity 79-93% specificity 0.960 AUROC		
J. Thomas et al (2018) [20]	scalp	CNN	0.935 AUROC		
J. Jing et al (2020) [15]	scalp	Split CNN (Temporal + Spatial convolutions)	0.98 AUROC		0.847 AUROC
Z. Xu et al (2021) [25]	scalp	LSTM	88.54% F1-score 92.04% sensitivity 85.75% precision		
B. Wei et al (2021) [27]	scalp	CNN + GRU	95.1% accuracy 93.8% sensitivity 96.8% specificity 95.4% F1-score 97.3% precision 0.973 AUROC		
M. C. Tjepkema-Cloostermans et al (2018) [16]	scalp	CNN + LSTM	47.4% sensitivity 98.0% specificity 0.94 AUROC	73% sensitivity (with 100% specificity)	83.33% specificity (12 recordings without IEDs)
K. Fukumori et al (2019) [21]	scalp	CNN, LSTM, GRU	0.768-0.942 AUROC		
F. Furbass et al (2020) [17]	scalp	Fast region-based CNN			88.89% sensitivity (54 recordings with IEDs) 69.57% specificity (46 recordings without IEDs)
R. J. Quon et al (2022) [24]	intracranial	CNN	95% F1-score 0.98 AUROC		
M. Abou Jaoude et al (2020) [23]	intracranial	CNN	84.0% sensitivity 0.996 AUROC	0.981 partial AUROC (with >90.0% specificity) 84% sensitivity (with <1/min FDR)	
A. Antoniades et al (2017) [22]	intracranial	CNN	85.92% accuracy 0.887 AUROC		
D.Geng et al (2021) [26]	intracranial	GRU	>93% accuracy >0.93 AUROC		

approaches using IEDs with various patterns [15], [16], [17], [18], [19], [20], [21], [22], [23], [24], [25], [26], [27] can detect IEDs caused by other types of epilepsy. However, their annotation processes are possibly more burdensome than the proposed approach. Therefore, we referred the previous studies presented in Table V to confirm that the proposed approach performed reasonable detection of CTSWs despite its simplified annotation process, instead of performing a direct comparison between their performances.

The proposed CNN architecture was similar to the ones previously proposed for IED detection [15] and task-related EEG decoding [35], [45]. It starts with a temporal convolution with a filter for each channel, followed by a spatial convolution with a filter for all channels, because temporal scalp EEG modulations have both local and global properties whereas spatial ones primarily only have the local property, which made us name the architecture a split CNN [35]. Presumably, there are two benefits of the split CNN: compared to a general 2D CNN, we can unmix globally spatial information using only a temporal filter; and compared to an image-based 2D CNN, we can reduce the dimensionality of input data [35]. However, we did not compare the detectability of the split CNN for CTSWs with those of other methods such as a CNN with a temporal filter [16], [18], [19], [20], [21], [22], [23], CNN using images as input data [24], fast region-based CNN [17], long short-term memory (LSTM) or gated recurrent unit [21], [25], [26], and hybrid CNN-LSTM [16], [27]. A previous study reported high IED detection performance

using the split CNN, with 0.980 and 0.847 AUROC for epoch- and EEG-level detections, respectively, [15]. The difference between our method and that used in the previous study [15] is that we used a split CNN to detect CTSWs and not IEDs with various patterns.

It has been reported that some normal features in sleep EEGs such as vertex sharp transients [46] and K-complexes [47], and non-physiological components such as electrostatic [48] and electrode pop [46] artifacts occasionally result in mislabeled IEDs [49], [50], [51], [52]. We observed that these normal EEG components and artifacts primarily resulted in false detections during the EEG-level detection. To reduce false detections, we suggest the following two strategies: EEG quality improvement and using a human in the loop of machine learning [53]. We observed the largest number of false detections in poor quality EEG recordings of controls (7 false detections by the fifth classification model) during EEG-level detection. With the accurate exclusion of these recordings based on the reviews of clinicians, a refined dataset can be constructed to retrain the current classification models. Thereafter, we expect that the retrained classification models will make fewer false detections in newly added EEG recordings than the current ones.

V. Conclusion

This study proposed a deep learning-based approach for automatically detecting CTSWs in scalp EEG recordings of patients with SLECTS. The proposed CNN-based CTSW detectors successfully discriminated CTSW-positive and CTSW-negative recordings with a sensitivity, specificity, and accuracy higher than 99%, 98%, and 99%, respectively, and an FDR of 0.19/hr. The proposed approach can only be used for CTSW detection. However, it can lower the burden of IED annotation on clinicians by limiting IEDs to CTSWs.

However, there are several limitations to this approach. First, we did not consider the bilateral property of CTSWs. We tried to identify the presence of CTSWs in the EEG recordings, without verifying whether they were located in the left or right hemisphere. Second, we did not quantify the amount of burden on clinicians that could be lowered during CTSW annotation. Third, we did not compare the performance of the proposed CTSW detectors with that of general IED detectors (trained using IEDs with various patterns) for the EEG-level detection.

To demonstrate the effectiveness and generalizability of the proposed approach, in a future work, we will test it using a new dataset, construct classification models using images obtained through a time-frequency transformation of EEG time series, adopt other deep learning architectures such as the hybrid CNN-LSTM, and perform multi-central EEG-level detection.

References

[1] B. S. Chang and D. H. Lowenstein, "Epilepsy," *New England J. Med.*, vol. 349, no. 13, p. 1257, Sep. 2003.

[2] R. S. Fisher, "Redefining epilepsy," *Current Opinion Neurol.*, vol. 28, no. 2, pp. 130–135, Apr. 2015.

[3] R. S. Fisher et al., "ILAE official report: A practical clinical definition of epilepsy," *Epilepsia*, vol. 55, no. 4, pp. 475–482, Apr. 2014.

[4] K. M. Fiest et al., "Prevalence and incidence of epilepsy: A systematic review and meta-analysis of international studies," *Neurology*, vol. 88, no. 3, pp. 296–303, Jan. 2017.

[5] T Vos et al., "Global, regional, and national incidence, prevalence, and years lived with disability for 310 diseases and injuries, 1990–2015: A systematic analysis for the global burden of disease study 2015," *Lancet*, vol. 388, pp. 1545–1602, Oct. 2016.

[6] J. S. Duncan, "Brain imaging in epilepsy," *Practical Neurol.*, vol. 19, no. 5, pp. 438–443, Oct. 2019.

[7] E. H. Middlebrooks, L. Ver Hoef, and J. P. Szaflarski, "Neuroimaging in epilepsy," *Current Neurol. Neurosci. Rep.*, vol. 17, no. 4, p. 32, Apr. 2017.

[8] R. J. Staba, M. Stead, and G. A. Worrell, "Electrophysiological biomarkers of epilepsy," *Neurotherapeutics*, vol. 11, no. 2, pp. 334–346, Apr. 2014.

[9] S. Noachtar and J. Rémi, "The role of EEG in epilepsy: A critical review," *Epilepsy Behav.*, vol. 15, pp. 22–33, May 2009.

[10] N. Kane et al., "A revised glossary of terms most commonly used by clinical electroencephalographers and updated proposal for the report format of the EEG findings. Revision 2017" *Clin. Neurophysiol. Pract.*, vol. 2, pp. 170–185, Jan. 2017.

[11] W. O. Tatum et al., "Clinical utility of EEG in diagnosing and monitoring epilepsy in adults," *Clin Neurophysiol*, vol. 129, no. 5, pp. 1056–1082, May 2018.

[12] S. B. Wilson and R. Emerson, "Spike detection: A review and comparison of algorithms," *Clin Neurophysiol*, vol. 113, no. 12, pp. 1873–1881, Dec. 2002.

[13] C. da Silva Lourenço, M. C. Tjepkema-Cloostermans, and M. J. A. M. van Putten, "Machine learning for detection of interictal epileptiform discharges," *Clin. Neurophysiol.*, vol. 132, no. 7, pp. 1433–1443, Jul. 2021.

[14] F. E. A. El-Samie, T. N. Alotaiby, M. I. Khalid, S. A. Alshebeili, and S. A. Aldosari, "A review of EEG and MEG epileptic spike detection algorithms," *IEEE Access*, vol. 6, pp. 60673–60688, 2018.

[15] J. Jing et al., "Development of expert-level automated detection of epileptiform discharges during electroencephalogram interpretation," *JAMA Neurol.*, vol. 77, no. 1, pp. 103–108, Oct. 2020.

[16] M. C. Tjepkema-Cloostermans, R. C. V. de Carvalho, and M. J. A. M. van Putten, "Deep learning for detection of focal epileptiform discharges from scalp EEG recordings," *Clin. Neurophysiol.*, vol. 129, no. 10, pp. 2191–2196, Oct. 2018.

[17] F. Fürbass, M. A. Kural, G. Gritsch, M. Hartmann, T. Kluge, and S. Beniczky, "An artificial intelligence-based EEG algorithm for detection of epileptiform EEG discharges: Validation against the diagnostic gold standard," *Clin. Neurophysiol.*, vol. 131, no. 6, pp. 1174–1179, Jun. 2020.

[18] S. Clarke et al., "Computer-assisted EEG diagnostic review for idiopathic generalized epilepsy," *Epilepsy Behav.*, vol. 121, Aug. 2021, Art. no. 106556.

[19] C. Lourenco, M. C. Tjepkema-Cloostermans, L. F. Teixeira, and M. J. van Putten, "Deep learning for interictal epileptiform discharge detection from scalp EEG recordings," in *Proc. 15th Medit. Conf. Med. Biol. Eng. Comput. (MEDICON)*, in IFMBE Proceedings, vol. 76. International Federation for Medical and Biological Engineering (IFMBE), 2020, pp. 1984–1997, doi: 10.1007/978-3-030-31635-8_237.

[20] J. Thomas, L. Comoretto, J. Jin, J. Dauwels, S. S. Cash, and M. B. Westover, "EEG CLassification via convolutional neural network-based interictal epileptiform event detection," in *Proc. 40th Annu. Int. Conf. IEEE Eng. Med. Biol. Soc. (EMBC)*, Jul. 2018, pp. 3148–3151.

[21] K. Fukumori, H. T. T. Nguyen, N. Yoshida, and T. Tanaka, "Fully data-driven convolutional filters with deep learning models for epileptic spike detection," in *Proc. IEEE Int. Conf. Acoust., Speech Signal Process. (ICASSP)*, May 2019, pp. 2772–2776.

[22] A. Antoniades et al., "Detection of interictal discharges with convolutional neural networks using discrete ordered multichannel intracranial EEG," *IEEE Trans. Neural Syst. Rehabil. Eng.*, vol. 25, no. 12, pp. 2285–2294, Dec. 2017.

[23] M. A. Jaoude et al., "Detection of mesial temporal lobe epileptiform discharges on intracranial electrodes using deep learning," *Clin. Neurophysiol.*, vol. 131, no. 1, pp. 133–141, Jan. 2020.

[24] R. J. Quon et al., "AiED: Artificial intelligence for the detection of intracranial interictal epileptiform discharges," *Clin. Neurophysiol.*, vol. 133, pp. 1–8, Jan. 2022.

[25] Z. Xu, T. Wang, J. Cao, Z. Bao, T. Jiang, and F. Gao, "BECT spike detection based on novel EEG sequence features and LSTM algorithms," *IEEE Trans. Neural Syst. Rehabil. Eng.*, vol. 29, pp. 1734–1743, 2021.

[26] D. Geng, A. Alkhachroum, M. A. M. Bicchi, J. R. Jagid, I. Cajigas, and Z. S. Chen, "Deep learning for robust detection of interictal epileptiform discharges," *J. Neural Eng.*, vol. 18, no. 5, Apr. 2021, Art. no. 056015.

[27] B. Wei, X. Zhao, L. Shi, L. Xu, T. Liu, and J. Zhang, "A deep learning framework with multi-perspective fusion for interictal epileptiform discharges detection in scalp electroencephalogram," *J. Neural Eng.*, vol. 18, no. 4, Jul. 2021, Art. no. 0460b3.
[28] Y. Hao, M. K. Hui, N. V. Ellenrieder, N. Zazubovits, and J. Gotman, "DeepIED: An epileptic discharge detector for EEG-fMRI based on deep learning," *Neuroimage Clin.*, vol. 17, pp. 962–975, Jan. 2018.
[29] S. Galicchio et al., "Self-limited epilepsy with centro-temporal spikes: A study of 46 patients with unusual clinical manifestations," *Epilepsy Res.*, vol. 169, Nov. 2020, Art. no. 106507.
[30] I. E. Scheffer et al., "ILAE classification of the epilepsies: Position paper of the ILAE commission for classification and terminology," *Epilepsia*, vol. 58, no. 4, pp. 512–521, Apr. 2017.
[31] W. D. Shields and O. C. Snead, "Benign epilepsy with centrotemporal spikes," *Epilepsia*, vol. 50, pp. 5–10, Sep. 2009.
[32] P. Kellaway, "The electroencephalographic features of benign centrotemporal (rolandic) epilepsy of childhood," *Epilepsia*, vol. 41, no. 8, pp. 1053–1056, Aug. 2000.
[33] C. Ilae, "Proposal for revised classification of epilepsies and epileptic syndromes," *Epilepsia*, vol. 30, no. 4, pp. 99–389, Aug. 1989.
[34] U. Kramer, "Atypical presentations of benign childhood epilepsy with centrotemporal spikes: A review," *J. Child Neurol.*, vol. 23, no. 7, pp. 785–790, Jul. 2008.
[35] R. T. Schirrmeister et al., "Deep learning with convolutional neural networks for EEG decoding and visualization," *Hum. Brain Mapping*, vol. 38, no. 11, pp. 5391–5420, Nov. 2017.
[36] K. He, X. Zhang, S. Ren, and J. Sun, "Deep residual learning for image recognition," in *Proc. IEEE Conf. Comput. Vis. Pattern Recognit. (CVPR)*, Jun. 2016, pp. 770–778.
[37] D. Lu and J. Triesch, "Residual deep convolutional neural network for EEG signal classification in epilepsy," 2019, *arXiv:1903.08100*.
[38] D.-A. Clevert, T. Unterthiner, and S. Hochreiter, "Fast and accurate deep network learning by exponential linear units (ELUs)," 2015, *arXiv:1511.07289*.
[39] N. Srivastava, G. Hinton, A. Krizhevsky, I. Sutskever, and R. Salakhutdinov, "Dropout: A simple way to prevent neural networks from overfitting," *J. Mach. Learn. Res.*, vol. 15, no. 1, pp. 1929–1958, 2014.
[40] S. Zagoruyko and N. Komodakis, "Wide residual networks," 2016, *arXiv:1605.07146*.
[41] S. Ioffe and C. Szegedy, "Batch normalization: Accelerating deep network training by reducing internal covariate shift," 2015, *arXiv:1502.03167*.
[42] K. He, X. Zhang, S. Ren, and J. Sun, "Delving deep into rectifiers: Surpassing human-level performance on ImageNet classification," in *Proc. IEEE Int. Conf. Comput. Vis. (ICCV)*, Dec. 2015, pp. 1026–1034.
[43] S. J. Reddi, S. Kale, and S. Kumar, "On the convergence of Adam and beyond," 2018, *arXiv:1904.0923*.
[44] A. Paszke et al., "PyTorch: An imperative style, high-performance deep learning library," in *Proc. Adv. Neural Inf. Process. Syst.*, vol. 32, 2019, pp. 1–12.
[45] R. T. Schirrmeister, L. Gemein, K. Eggensperger, F. Hutter, and T. Ball, "Deep learning with convolutional neural networks for decoding and visualization of EEG pathology," 2017, *arXiv:1708.08012*.
[46] S. D. Kara, U. Amin, and S. R. Benbadis, "Reversing the myth of phase reversals," *Expert Rev. Neurotherapeutics*, vol. 20, no. 1, pp. 3–5, Jan. 2020.
[47] S. Kohsaka, T. Sakai, M. Kohsaka, N. Fukuda, and T. Ariga, "Activation of the brainstem precedes and outlasts the K-complex in humans," *Neuroscience*, vol. 202, pp. 243–251, Jan. 2012.
[48] W. O. Tatum, B. A. Dworetzky, and D. L. Schomer, "Artifact and recording concepts in EEG," *J. Clin. Neurophysiol.*, vol. 28, no. 3, pp. 252–263, Jun. 2011.
[49] W. O. Tatum, "Normal 'suspicious' EEG," *Neurology*, vol. 80, no. 1, pp. S4–S11, Jan. 2013.
[50] W. O. Tatum, "How not to read an EEG: Introductory statements," *Neurology*, vol. 80, no. 1, pp. S1–S3, Jan. 2013.
[51] S. R. Benbadis, "Misdiagnosis of epilepsy due to errors in EEG interpretation," *Practical Neurol.*, vol. 7, no. 5, pp. 323–325, Oct. 2007.
[52] S. R. Benbadis, "Errors in EEGs and the misdiagnosis of epilepsy: Importance, causes, consequences, and proposed remedies," *Epilepsy Behav.*, vol. 11, no. 3, pp. 257–262, Nov. 2007.
[53] A. Holzinger, "Interactive machine learning for health informatics: When do we need the human-in-the-loop?" *Brain Informat.*, vol. 3, no. 2, pp. 119–131, Jun. 2016.